DETAILS OF CATCHMENTS STUDIED

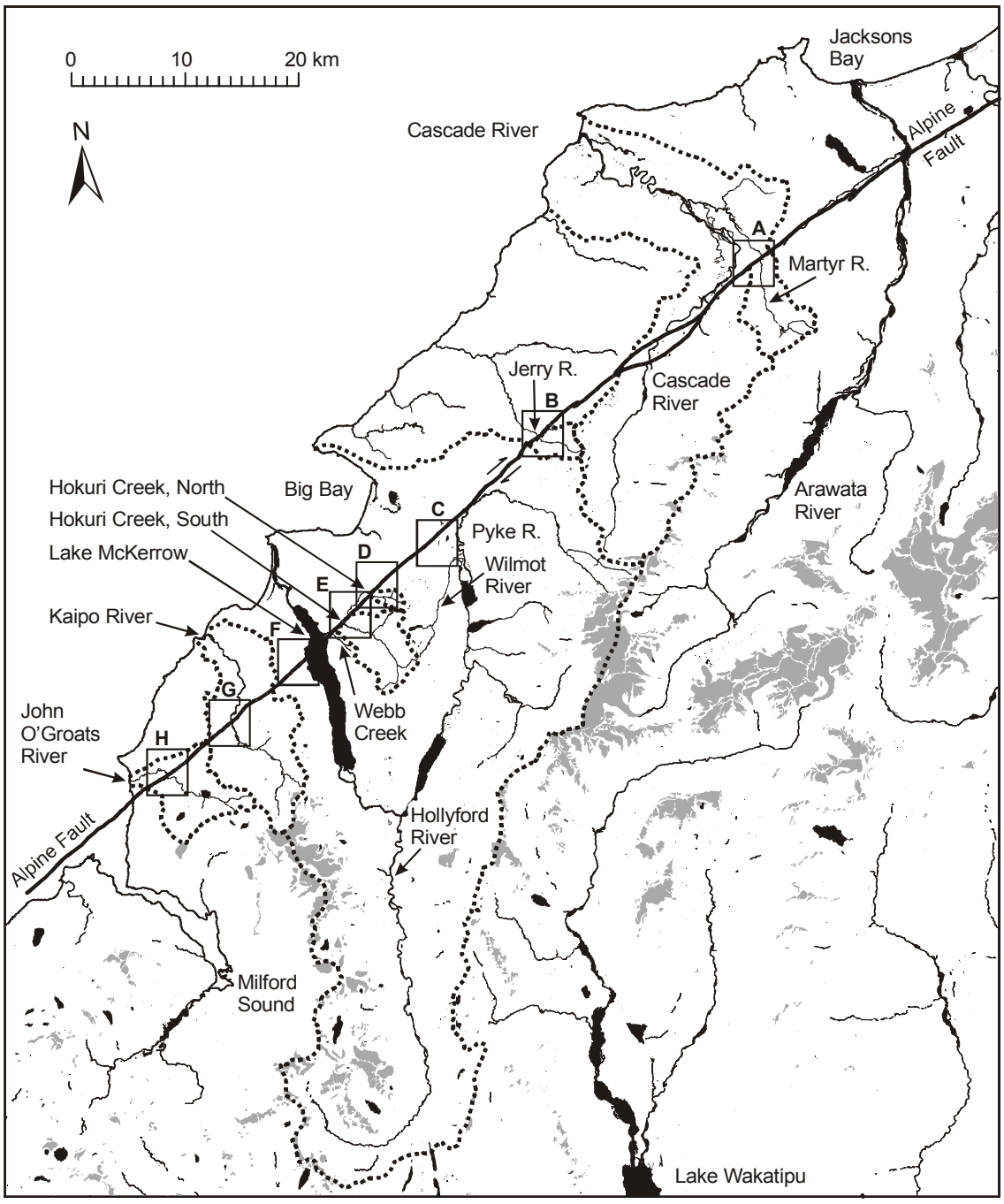

Figure DR1. Catchment boundaries (bold dotted lines) and locations of offset features (main text Fig. 3A-H). Areas of permanent snow and ice cover are shaded. Lakes and active river beds are shown black.

TABLE DR1. CATCHMENTS STUDIED.

Name	Area (km^2)	Highest peak (m)	Longest river (km)
Cascade River	402	1951	50
Martyr River*	33	1683	8
Jerry River*	10	1306	4
Hokuri Creek, North Branch*	3	1330	3
Hokuri Creek, South Branch*	30	1507	10
Lake McKerrow-Big Bay	1200	2723	70
Kaipo River	106	2134	22
John O'Groats River	45	2015	12

*only catchment southeast of Alpine fault is considered.

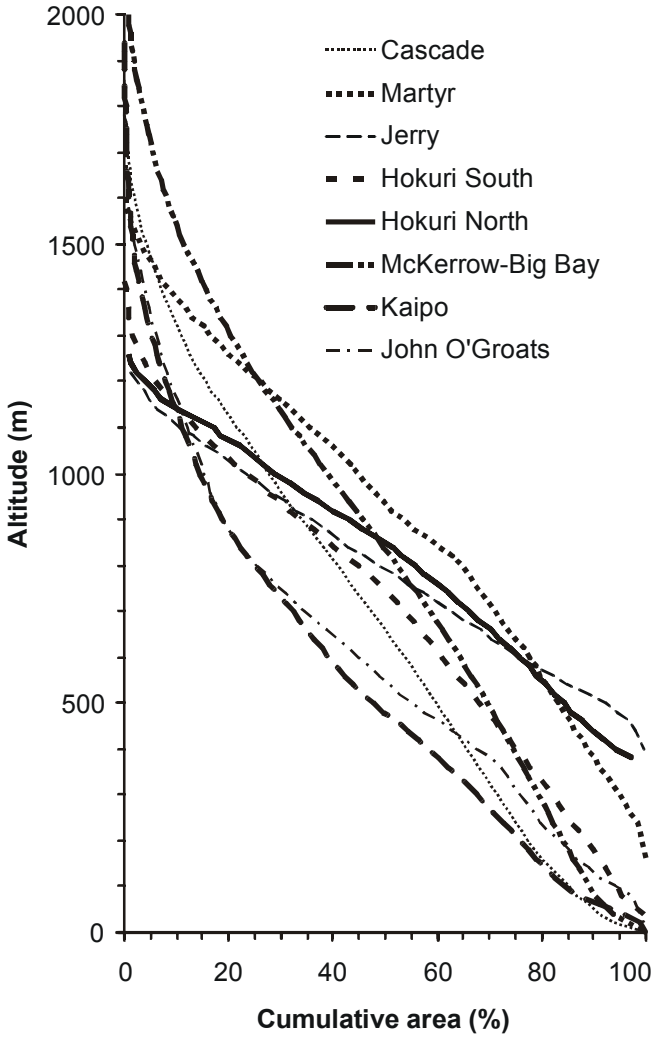

Figure DR2. Hypsometry of catchments studied.

ALPINE FAULT AERIAL-OBLIQUE PHOTOS

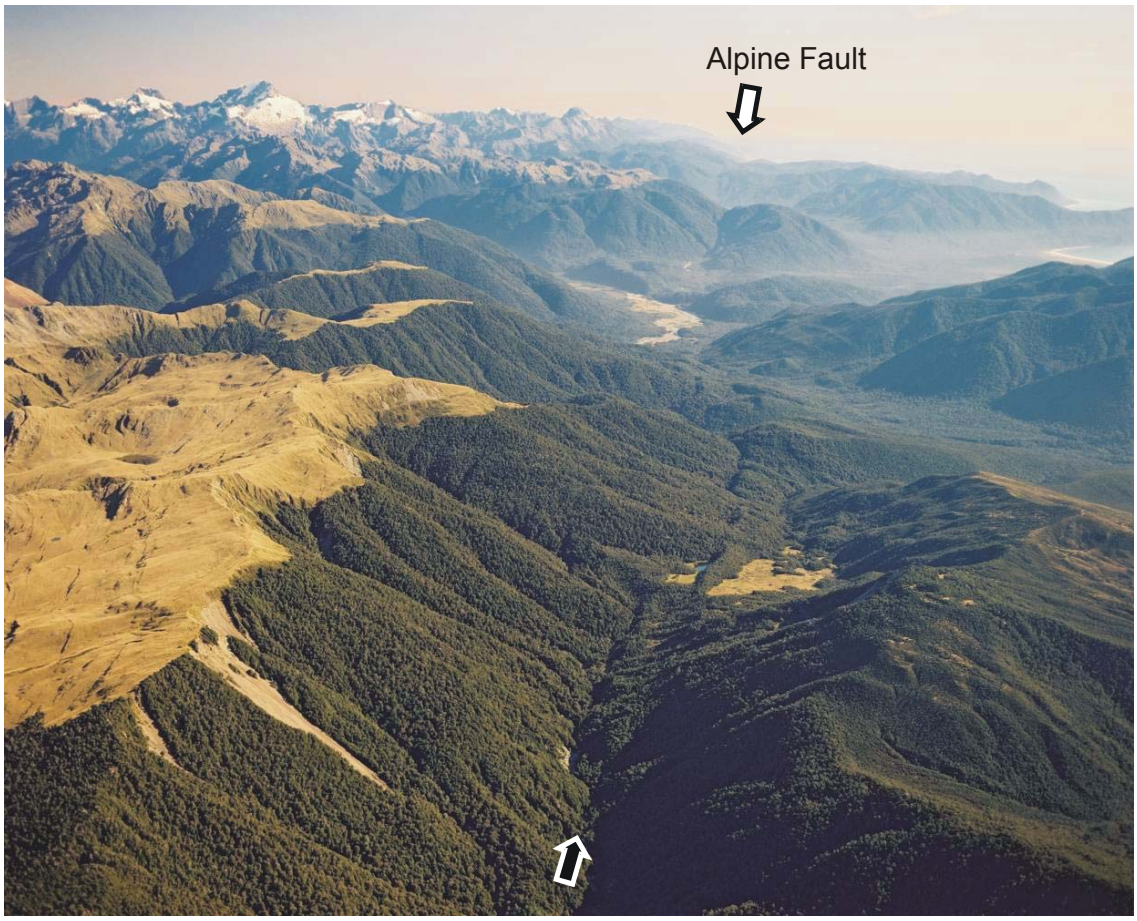

Figure DR3. View southwest along the Alpine Fault trace across the heavily forested Jerry River and upper Pyke river valleys. The upper limit of forest is at an altitude of approximately 1000 m. A right-step in the fault trace and small pull-apart lake is visible in the foreground. The offset northern end of the Skippers Range and the coast at Big Bay is visible in the middle distance. Snowy peaks of the Darran Mountains (top left) feed the Hollyford, Kaipo, and John O'Groats rivers. Photo: D.L. Homer. Copyright Institute of Geological & Nuclear Sciences.

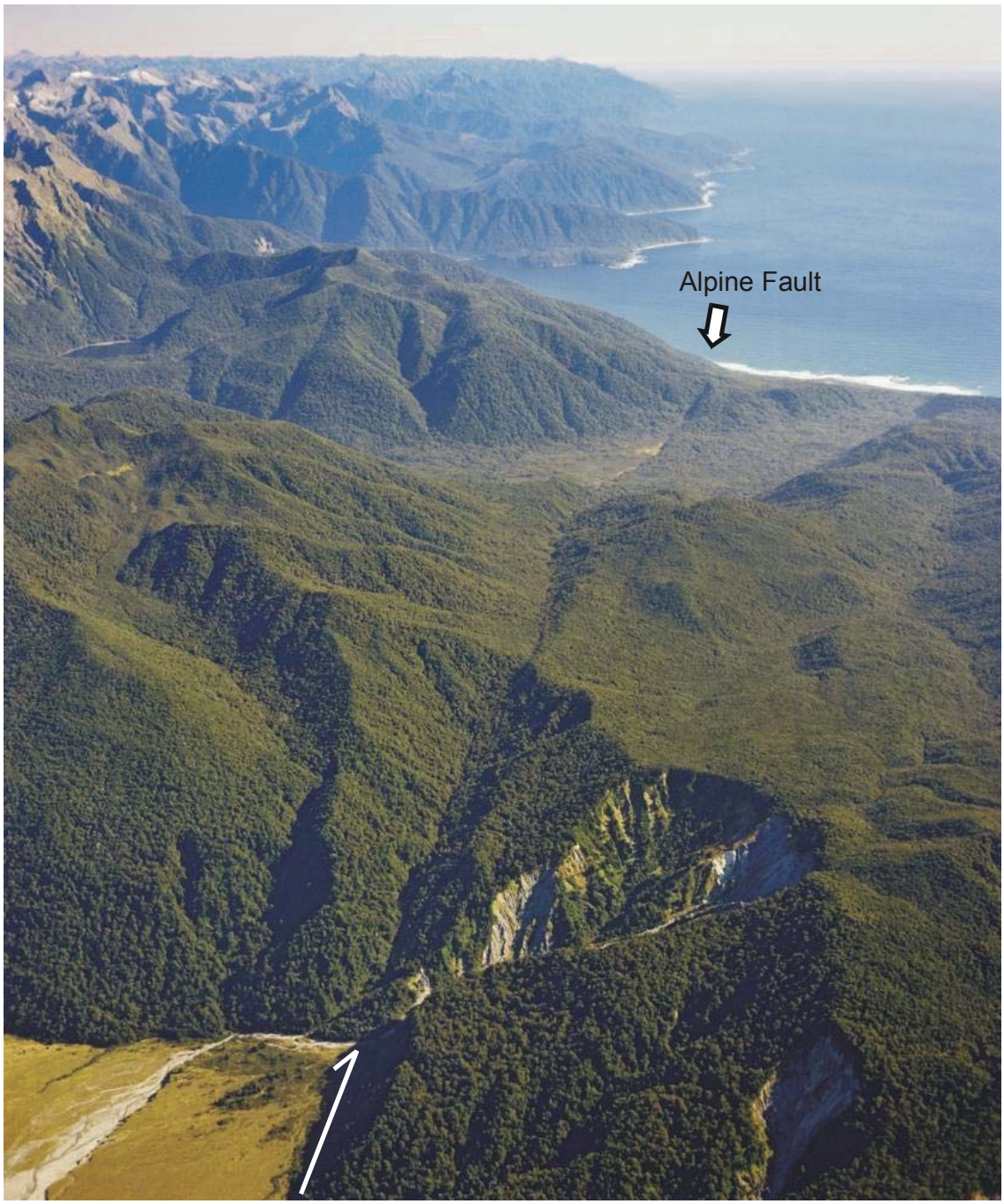

Figure DR4. View southwest along the Alpine Fault trace across the heavily forested Kaipo (foreground) and John O'Groats river valleys to where the fault trace crosses the coast at Milford Sound. Photo: D.L. Homer. Copyright Institute of Geological & Nuclear Sciences.

COSMOGENIC ISOTOPE DATA

A companion study (full details to be published elsewhere) analysed boulders embedded in lateral moraines of the Cascade Plateau (main text Fig. 2). Cosmogenic isotope ages from the companion study that are significant to this study are detailed in Table DR2.

Analytical work was carried out by Kyeong Kim (now at Institute of Meteorics, University of New Mexico, Albuquerque, NM 87131, USA) and Albert Zondervan while employed by the Institute of Geological & Nuclear Sciences (GNS) in Lower Hutt, NZ. Samples 1, 4, 7, and 8 were processed and measured using Accelerator Mass Spectrometry (AMS) at the GNS National Isotope Centre in Lower Hutt. Sample 6 was submitted for wet chemistry at PrimeLab, Purdue University (Indiana, USA). Blank 1 was produced at GNS and blank 4 at PrimeLab. Column 5 of Table DR2 is the combined result of the AMS measurements on samples and blanks.

TABLE DR2. SELECTED COSMOGENIC ISOTOPE DATA FROM CASCADE PLATEAU

Sample number	Altitude (m)	^{10}Be surface production rate (atom g^{-1} yr^{-1})	AMS code (blank used)	^{10}Be/^{9}Be (10^{-15})	^{10}Be concentration (10^{4} atom g^{-1})	Age
1	390	7.15	Be-1764 (1)	354 ± 15	39.2 ± 1.8	57.8 ± 2.7
4	390	7.15	Be-1767 (1)	693 ± 19	53.3 ± 1.6	79.1 ± 2.3
6	405	7.25	Be-1943 (4)	995 ± 24	53.0 ± 1.4	77.5 ± 2.0
7	370	7.03	Be-1769 (1)	467 ± 15	52.4 ± 1.8	79.1 ± 2.8
8	370	7.03	Be-1770 (1)	471 ± 29	53.0 ± 3.4	79.9 ± 5.2
			Be-1761 (blank-1)	21 ± 3		
			Be-1946 (blank-4)	6 ± 9		

The surface-exposure age calculation accounts for altitude and geomagnetic-latitude (Stone, 2000) and uses a high-latitude sea-level ^{10}Be production rate of 5.1 atom (g SiO2)$^{-1}$ a^{-1}. The reduction in ^{10}Be production rate across the depth interval of sampling was calculated using an exponential expression for attenuation of fast neutrons, with attenuation length 165 g cm^{-2} and average rock density 2.7 g cm^{-3}. All samples were from a 0-5 cm depth interval, resulting in a 4% attenuation correction. We have chosen to introduce a 0.1% random error with the 4% attenuation, to take into account a 1% uncertainty in attenuation length and average rock density, and a 2% error in the measurement of the sampling depth. Obstruction of fast cosmogenic neutrons by nearby hills is negligible. The radiometric half-life of ^{10}Be was assumed to be 1.51 Ma. Inheritance of ^{10}Be from prior exposure was assumed to be zero.

STATISTICAL TREATMENT OF DISPLACEMENT RATE DATA

The joint probability density, $\gamma(x)$, at offset x is the product of the n individual probability densities, $p_i(x)$, normalised so that the total joint probability is equal to 1.

$$\gamma(x) = \frac{\prod_{i=1}^{n} p_i(x)}{\int_{-\infty}^{\infty}\left(\prod_{i=1}^{n} p_i(x)\right)\mathrm{d}x}$$

The weighted mean, μ_w, is weighted such that each observation contributes equally to the variance, and the sum of the weights is equal to 1.

$$\mu_w = \sum_{i=1}^{i=n} w_i x_i$$

$$w_i = \frac{C_{xi}^{-2}}{\sum_{i=1}^{n} C_{xi}^{-2}}$$

where w_i is the weight, x_i is the measured offset, and C_{xi} is the respective confidence interval half-width (which is linearly proportional to the standard deviation) for the *i*th observation (locality).

The arithmetic mean, μ_a, is given by

$$\mu_a = \frac{1}{n}\sum_{i=1}^{n} x_i$$

The probability distributions for the weighted and arithmetic means were found by a Monte-Carlo method. The offset distributions were randomly sampled (assumed independent) and the mean taken, and the process was repeated until the probability density of the mean was sufficiently precisely determined.

Eight sites with rank 1 offsets were identified in this analysis. The weighted mean offset is 416 m, with standard deviation of the mean of 8.1 m, but two sites contribute a combined weight of 80% toward the mean value. The arithmetic mean offset is 435 m, with standard deviation of the mean of 15.3 m (Fig. DR5). Standard deviations of the weighted and arithmetic means were computed from the individual probability density functions ie. by propagation of measurement uncertainties. In comparison, the estimated standard error of the arithmetic mean, computed only from the variation in mean estimates for each site (ie. ignoring C_x values and looking only at the variation in mean value between sites) is 9.2 m. If the eight best-estimates are considered equally likely, and were taken from the same distribution, then the distribution of the arithmetic mean can be inferred from a Student's t-distribution with seven degrees of freedom and standard error 9.2 m. It can be seen from Figure DR5 that the t-distribution has comparable variance to the weighted mean and smaller variance than the numerically-determined distribution of the arithmetic mean (ie. the variance expected from inferred measurement precision). It can be concluded that the variation in offset values from different sites is less than would be expected from taking the arithmetic mean of the individual probability density functions (ie. propagation of measurement uncertainty). This is unsurprising, because the rectangular probability density functions assumed for offset at each locality likely under-estimate probabilities of offset near to the median value and over-estimate probabilities near the bounding values.

The implications of alternative methods for combining rank 1 data are shown graphically in Figure DR5. Implicit in the joint probability method is the assumption that there is no real variation in offset between sites; the method is very sensitive to observations that contain bias. The underlying assumption may be untrue, because some real variation in offset may exist between sites, and bias is likely due to local throw on the fault or misinterpretation of post-glacial landslide or fluvial morphology. For this reason, we choose not to combine offset data using joint probability. The weighted mean method is a better combined estimator of mean and variance. However, it is inefficient, because the weighting scheme inevitably results in a relatively small number of measurements contributing a large weight. The method also relies heavily on the assumption that the variance of the observation is accurately known. In fact, C_x has been estimated from data and is itself subject to substantial (unknown) uncertainty.

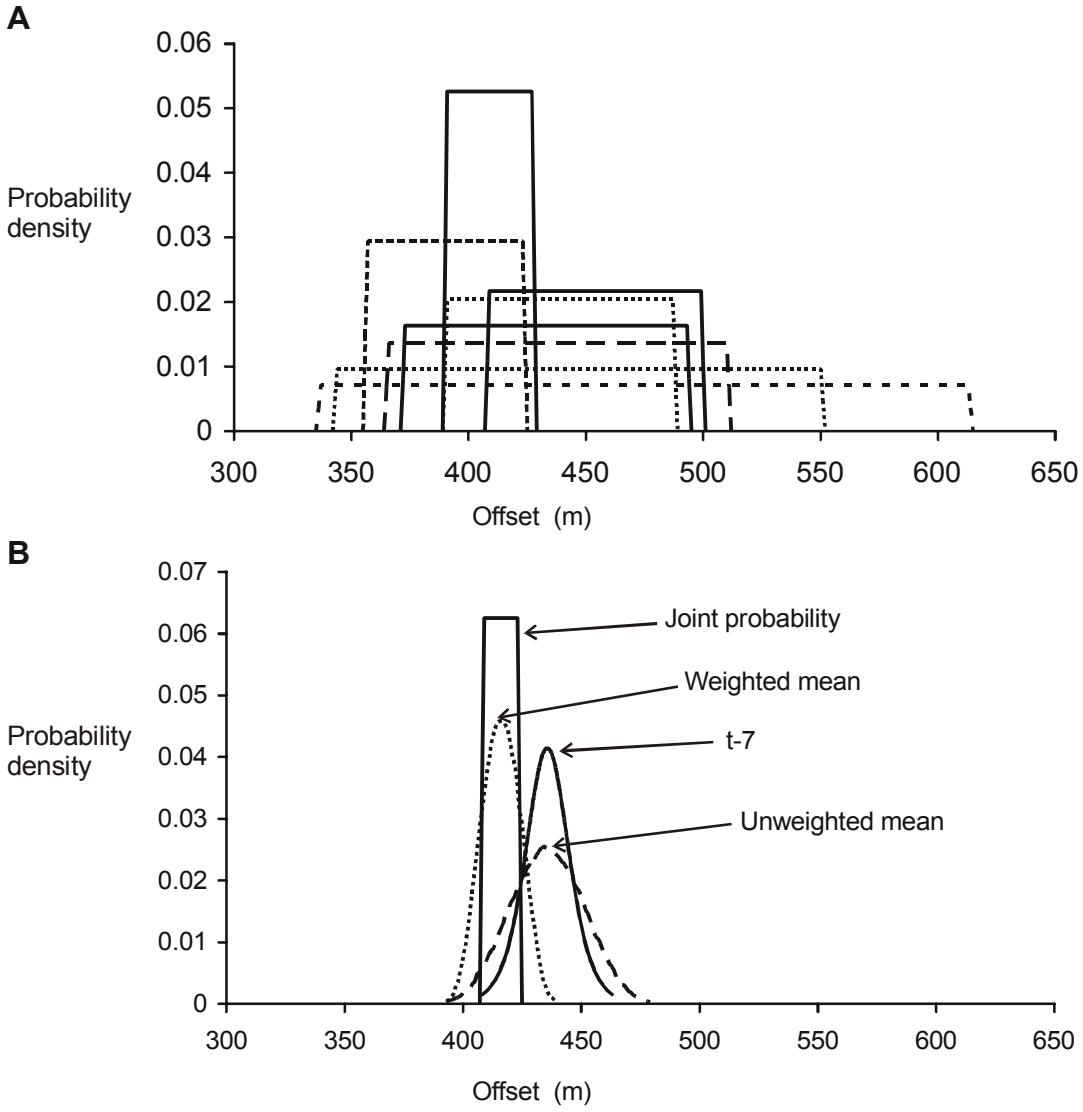

Figure DR5. A, probability density functions assumed for offset at each of the eight rank 1 sites (see main text). B, probability density functions for the weighted mean, joint probability, and arithmetic (unweighted) mean. It is assumed that observations between sites are independent. Also shown is a Student's t-distribution with 7 degrees of freedom, with mean and standard error derived from the eight rank 1 best-estimate offsets.

We choose to combine offset data by rank using an arithmetic mean. This is because the sample sizes are small, and because systematic effects tend to efficiently cancel between sites (opposite sides of a valley are typically oppositely affected by fault throw or erosion-deposition events). The procedure is the most efficient and is least sensitive to inappropriate assumptions (real offset differences, bias introduced by fault throw or erosion-deposition, and poor estimation of C_x).

Probability density functions for displacement rate computed for each rank are shown in Figure DR6A. These were computed using a Monte-Carlo approach where the offset distribution (combined by rank) and rectangular age distribution of width $2C_t$ (see main text) were randomly sampled ie. no age-offset correlation assumed within the same rank. The combined results are shown in Figure DR6B.

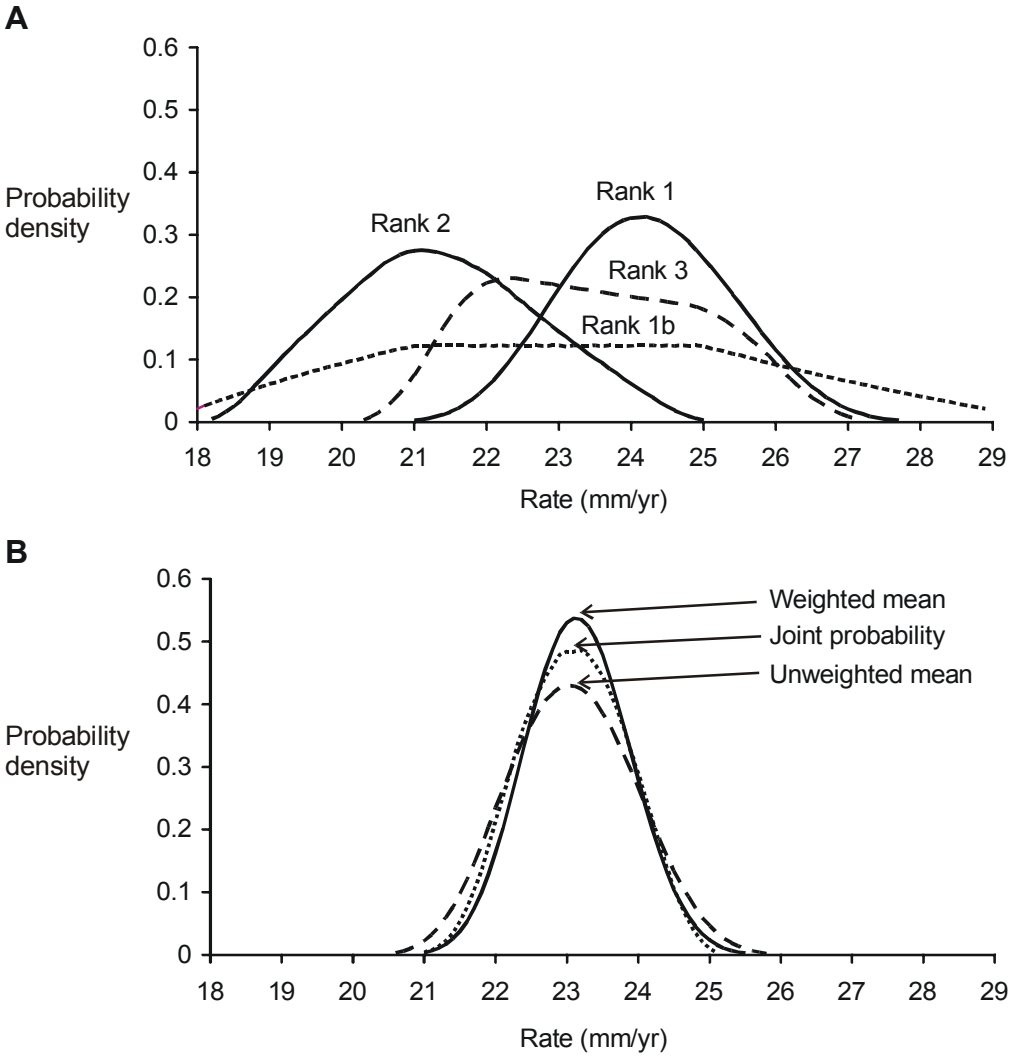

Figure DR6. A, probability density functions for displacement rate calculated from each rank, assuming uniform probability within specified confidence intervals of offset and age, and no correlation between offset and age within ranks (see main text). B, probability density functions for the weighted mean, joint probability, and arithmetic (unweighted) mean of displacement rates pooled by rank. It is assumed that rates derived from different ranks are independent.

SOUTH ISLAND KINEMATIC MODEL - COLOR

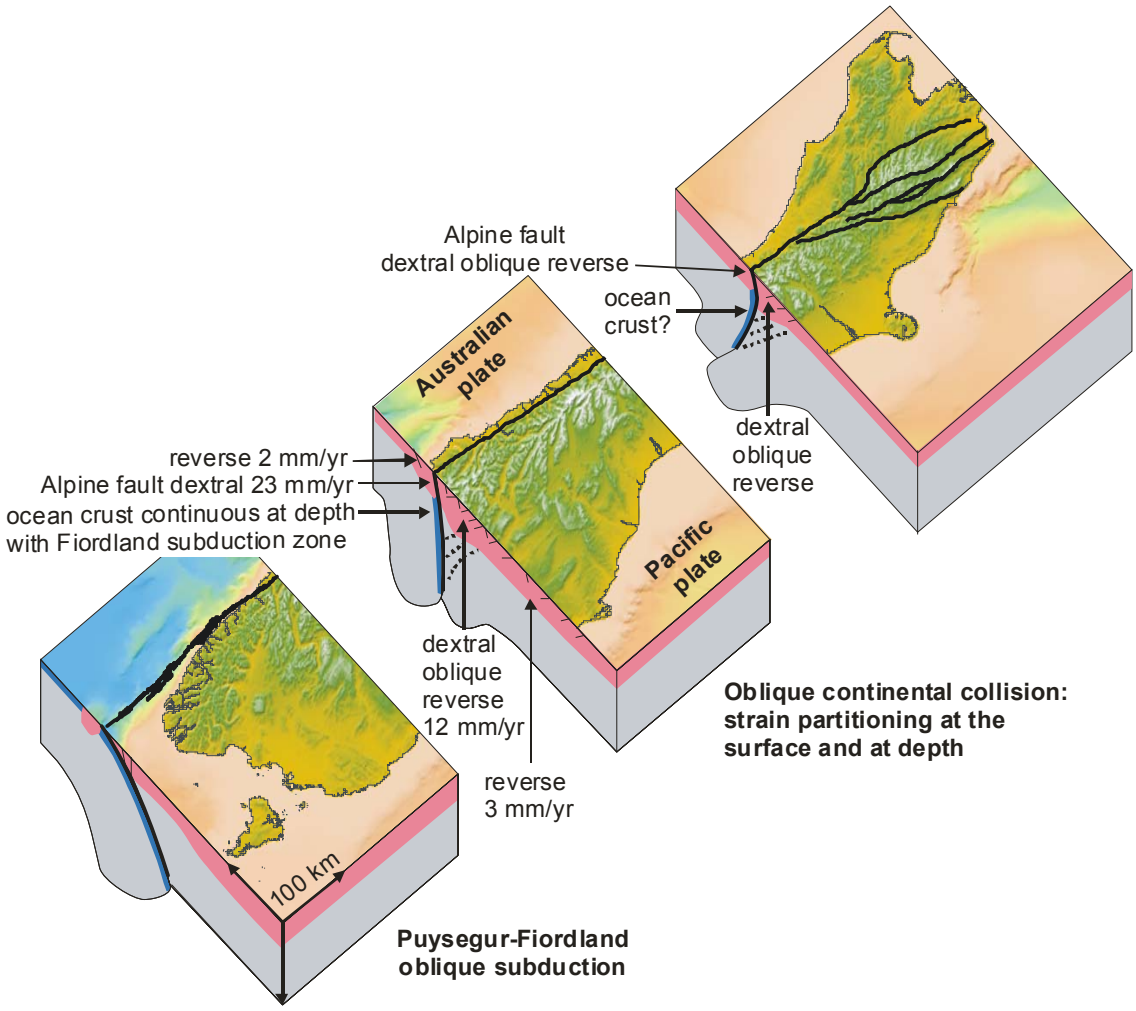

Figure DR7. Color version of kinematic model (main text Fig. 7).

SOUTH ISLAND KINEMATIC MODEL – COLOR, NO TEXT

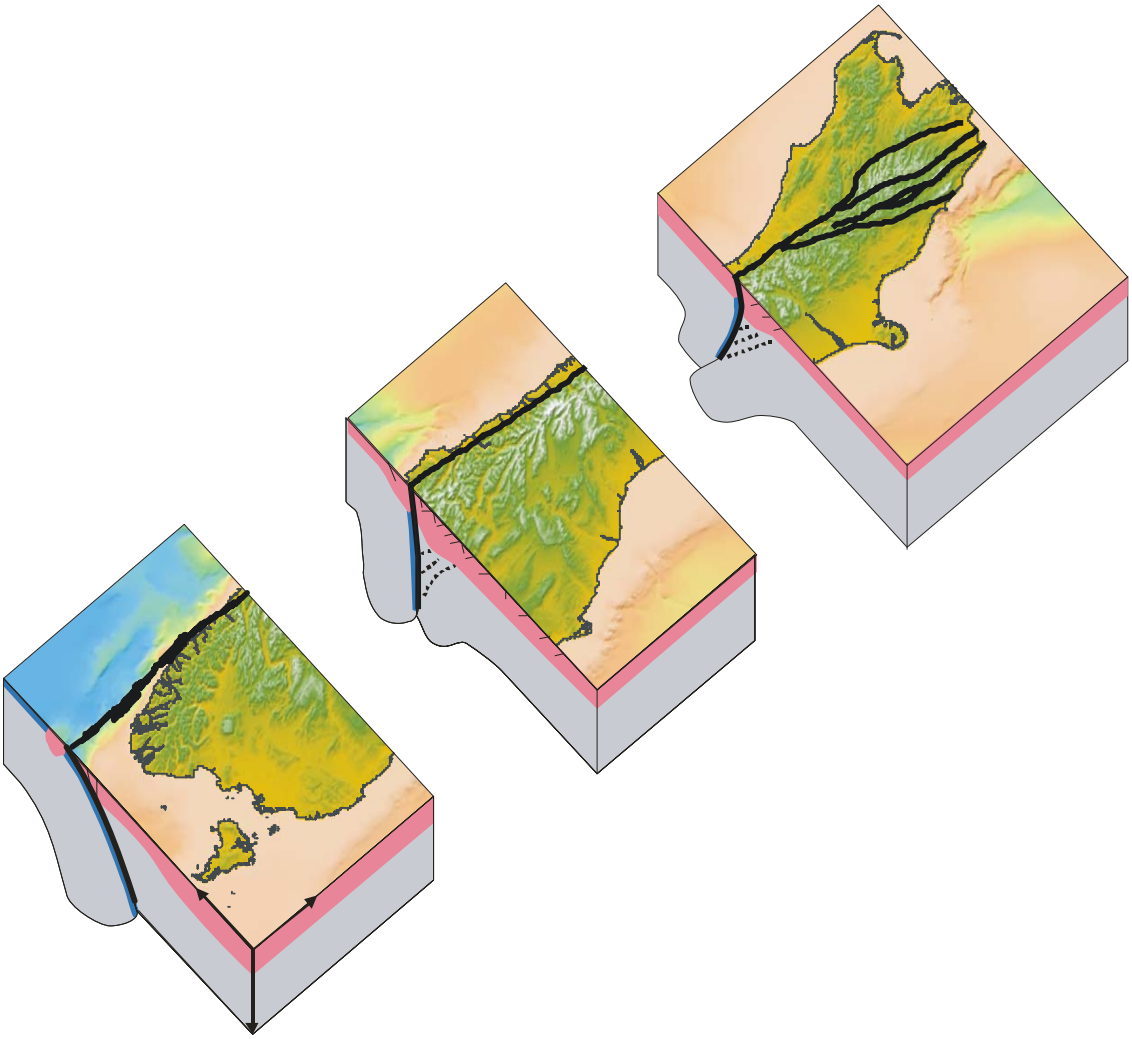

Figure DR8. Color version of kinematic model, with text omitted (main text Fig. 7).

SEISMIC HAZARD REDETERMINATION

TABLE DR3. REVISED PROBABILITY OF RUPTURE ON THE SOUTHERN ONSHORE ALPINE FAULT DURING TIME INTERVALS STARTING IN 2002.

Model	Probability in specified time interval			
	1 yr	20 yr	50 yr	100 yr
Exponential	0.0029	0.057	0.14	0.25
Lognormal	0.0066	0.12	0.28	0.47
Weibull	0.0067	0.13	0.29	0.54
Inverse.Gaussian	0.0048	0.093	0.22	0.39

Note: This table can be compared directly to Table 3 of Rhoades and Van Dissen (2003), and is based upon additional published data (Rhoades and Van Dissen, 2003).

REFERENCES CITED

Rhoades, D. A., and Van Dissen, R. J., 2003, Estimates of time-varying hazard of rupture of the Alpine Fault, New Zealand, allowing for uncertainties: New Zealand Journal of Geology and Geophysics, v. 46, no. 479-488.

Stone, J. O., 2000, Air pressure and cosmogenic isotope production: Journal of Geophysical Research, B, Solid Earth and Planets, v. 105, no. 10, p. 23,753-23,759.